JOURNAL OF VIROLOGY, July 2011, p. 6416–6426 Vol. 85, No. 13
0022-538X/11/$12.00 doi:10.1128/JVI.01500-10

Entry of Tiger Frog Virus (an Iridovirus) into HepG2 Cells via a pH-Dependent, Atypical, Caveola-Mediated Endocytosis Pathway▽

Chang-Jun Guo,[1,2]† Dong Liu,[2]† Yan-Yan Wu,[2] Xiao-Bo Yang,[2] Li-Shi Yang,[2] Shu Mi,[2] Yu-Xin Huang,[2] Yong-Wen Luo,[2] Kun-Tong Jia,[2] Zhao-Yu Liu,[2] Wei-Jian Chen,[2] Shao-Ping Weng,[2] Xiao-Qiang Yu,[3] and Jian-Guo He[1,2]*

MOE Key Laboratory of Aquatic Product Safety/State Key Laboratory for Biocontrol, School of Life Sciences, Sun Yat-sen University, 135 Xingang Road West, Guangzhou 510275, People's Republic of China[1]; School of Marine, Sun Yat-sen University, 135 Xingang Road West, Guangzhou 510275, People's Republic of China[2]; and Division of Cell Biology and Biophysics, School of Biological Sciences, University of Missouri—Kansas City, Kansas City, Missouri 64110[3]

Received 19 July 2010/Accepted 23 March 2011

Tiger frog virus (TFV), in the genus *Ranavirus* of the family *Iridoviridae*, causes high mortality of cultured tiger frog tadpoles in China. To explore the cellular entry mechanism of TFV, HepG2 cells were treated with drugs that inhibit the main endocytic pathways. We observed that TFV entry was inhibited by NH_4Cl, chloroquine, and bafilomycin, which can all elevate the pH of acidic organelles. In contrast, TFV entry was not influenced by chlorpromazine or overexpression of a dominant-negative form of Esp15, which inhibit the assembly of clathrin-coated pits. These results suggested that TFV entry was not associated with clathrin-mediated endocytosis, but was related to the pH of acidic organelles. Subsequently, we found that endocytosis of TFV was dependent on membrane cholesterol and was inhibited by the caveolin-1 scaffolding domain peptide. Dynamin and actin were also required for TFV entry. In addition, TFV virions colocalized with the cholera toxin subunit B, indicating that TFV enters as caveola-internalized cargo into the Golgi complex. Taken together, our results demonstrated that TFV entry occurs by caveola-mediated endocytosis with a pH-dependent step. This atypical caveola-mediated endocytosis is different from the clathrin-mediated endocytosis of frog virus 3 (FV3) by BHK cells, which has been recognized as a model for iridoviruses. Thus, our work may help further the understanding of the initial steps of iridovirus infection in lower vertebrates.

Every virus infection begins with entry of the virus into the host cell. Animal viruses are now accepted to have evolved a number of ways to effect their entry into host cells (11). In principle, three general entry pathways exist for viruses: direct fusion of the viral envelopes of some enveloped viruses with the plasma membrane, endocytosis by some enveloped and nonenveloped viruses, and direct translocation of nonenenveloped viral particles into the cytoplasm (2, 28). With respect to endocytosis, a number of different endocytotic pathways have been characterized, including clathrin-mediated endocytosis, caveola-mediated and dynamin-dependent endocytosis, macropinocytosis, and the less-well-studied clathrin-, caveola- and dynamin-independent endocytoses (37, 63). Among these pathways, the distinct receptor-mediated endocytosis pathways for virus entry via clathrin and caveolae are the best understood (5, 53).

Clathrin-mediated endocytosis is the most thoroughly characterized pathway and is considered to represent the primary route of endocytic entry into cells (33). Viruses bound to their receptor(s) are endocytosed and then transported to the early endosomes, which are acidic organelles and which become more acidic as they mature to form late endosomes (23). This acidification of endosomes is required for establishment of viral infection (32, 66). Many enveloped and nonenveloped viruses are known to employ the clathrin-mediated endocytosis pathway for their entry into host cells, including influenza virus (53), West Nile virus (9), African swine fever virus (21), Hantaan virus (25), dengue virus serotype 2 (47), rubella virus (26), and the polyomavirus JC virus (JCV) (49), among others.

Recently, another endocytic mechanism, namely, caveola-mediated endocytosis, has been described for the entry of many viruses. Caveolae are specialized flask-shaped invaginations of the plasma membrane. They are highly enriched in glycosphingolipids and cholesterol and are characterized by the presence of caveolin protein, a 20- to 24-kDa integral membrane protein (61). In contrast to clathrin-mediated endocytosis, the internalization of caveolae is a signal-triggered event. Triggering can occur by clustering of lipid raft components on the plasma membrane into caveolae, and invagination and internalization of caveolae are mediated by signal transduction pathways (44). Subsequently, the caveolar vesicles are delivered to the caveosomes, which are preexisting cholesterol- and caveolin-1-enriched organelles with a neutral pH. From there, they are transported to the endoplasmic reticulum (50). Caveola-dependent endocytosis was originally identified as an entry pathway for simian virus 40 (SV40) (45). Since then, the use of caveolae for entry into host cells has been demonstrated for other viruses, such as amphotropic murine leukemia virus

* Corresponding author. Mailing address: State Key Laboratory for Biocontrol, School of Life Sciences, Sun Yat-sen University, 135 Xingang Road West, Guangzhou 510275, People's Republic of China Phone: 86 20 3933 2988. Fax: 86 20 3933 2849. E-mail: lsshjg@mail.sysu.edu.cn.

† These authors contributed equally to this work.

▽ Published ahead of print on 4 May 2011.

(2), enterovirus (57), coronavirus 229E (41), and foot-and-mouth disease virus (42), among others. Different endocytotic pathways for virus entry can be distinguished by inhibiting endocytotic internalization with various drugs or by use of dominant-negative mutants of key proteins (56).

Iridoviruses are large icosahedral cytoplasmic DNA viruses that contain circularly permutated and terminally redundant double-stranded DNA genomes (10, 14). The current members of the family *Iridoviridae* are divided into five genera: *Iridovirus*, *Chloriridovirus*, *Ranavirus*, *Lymphocystivirus*, and *Megalocytivirus* (7, 24). The tiger frog virus (TFV) has been isolated from the diseased tadpoles of the frog *Rana tigrina rugulosa*, and it causes high mortality of tiger frog tadpoles cultured in southern China (65). The first complete genome sequence reported in the genus *Ranavirus* was that of TFV (19). The deduced amino acid sequences of TFV gene products show more than 90% identity to those of frog virus 3 (FV3), a type species of the genus *Ranavirus* (34, 59).

In the present study, we used different approaches to investigate the main internalization mechanism resulting in TFV entry into HepG2 cells. The entry of TFV appears to be an atypical caveola-mediated endocytosis pathway, which differs from the classical clathrin-mediated endocytosis pathway used by FV3. Our findings may further the understanding of the initial steps of iridovirus infection in lower vertebrates.

MATERIALS AND METHODS

Cells and virus. HepG2 cells (ATCC HB8065) were cultured in complete Dulbecco's modified Eagle's medium (DMEM) supplemented with 10% fetal bovine serum and were used for all experiments carried out in this work. The TFV was originally isolated from diseased tiger frog (*Rana tigrina rugulosa*) tadpoles in Naihai, Guangdong, China, and was maintained by our lab. TFV was propagated on confluent monolayers of FHM cells grown in 75-cm^2 flasks and incubated in DMEM containing 10% fetal bovine serum (FBS). To generate virus stocks, FHM cells were infected with TFV suspension and harvested ~5 days later when the cytopathic effect was marked. Virions were released by three freeze-thaw cycles and clarified by low-speed centrifugation. To determine virus titer, cells were grown in 96-well culture plates until 90% confluence. Virus titers were calculated by using a 50% endpoint method using the 50% tissue culture infective dose ($TCID_{50}$) (67). Virus suspensions at a multiplicity of infection (MOI) of 10 were used in our study.

Antibodies and reagents. Mouse polyclonal serum against TFV membrane protein ORF020R was prepared according to a method described previously (64). Rabbit anti-β-tubulin monoclonal antibody was purchased from Epitomics, Inc. (Burlingame, CA). Rabbit anti-green fluorescent protein (anti-GFP) polyclonal antibody and cell counting kit 8 (CCK-8) were from Beyotime Biotechnology, Inc. (Jiangsu, China). Goat anti-mouse IgG and goat anti-rabbit IgG conjugated with alkaline phosphatase were purchased from Promega (Madison, WI). Alexa Fluor 488-labeled goat anti-mouse IgG, Alexa Fluor 555-conjugated cholera toxin subunit B (CTxB-AF555), and Alexa Fluor 555-conjugated transferrin (Tf-AF555) were from Invitrogen Corporation (Carlsbad, CA). NH_4Cl, chloroquine (CQ), chlorpromazine (CPZ), methyl-β-cyclodextrin (MβCD), bafilomycin A1 (Baf.A1), cholesterol, genistein, dynasore, and cytochalasin B (CytoB) were purchased from Sigma-Aldrich (St. Louis, MO). Okadaic acid was purchased from Beyotime Biotechnology, Inc. (Jiangsu, China). Caveolin-1 scaffolding domain peptide (caveolin-1 peptide), corresponding to full-length caveolin-1 (amino acids 82 to 101) and synthesized as a fusion peptide to the C terminus of the *Antennapedia* internalization sequence, was purchased from Calbiochem (San Diego, CA). An irrelevant peptide (WGVDKASFTTFTVTK YWCRY) as a control peptide was synthesized as a fusion peptide to the C terminus of the *Antennapedia* internalization sequence by standard fluorenylmethoxycarbonyl chemistry and analyzed by mass spectrometry to confirm purity by the Sangon Biological Engineering Technology & Service Co., Ltd. (Shanghai, China).

Virus-infected HepG2 cells. Confluent monolayers of HepG2 cells in 48-well plates (for immunofluorescence or reverse transcription-PCR [RT-PCR] assay) or 6-well plates (for Western blot analysis) were infected with TFV (MOI of 10) and incubated at 27°C for 60 min. After adsorption, the virus inoculum was removed. Cells were washed twice with phosphate-buffered saline (PBS), and DMEM was added. The infections were allowed to proceed for 72 h at 27°C, and then levels of expression of ORF020R were determined.

Transcriptional analysis of TFV infection. HepG2 cells were infected with TFV as described above. Total RNA was isolated with TRIzol reagent (Invitrogen, CA), and cDNAs were prepared according to a method reported previously (17). The mRNA expression of the major capsid protein (*mcp*) gene and membrane protein ORF020R gene was determined as described previously (64).

Western blot analysis. Cells were harvested and lysed with a modified radioimmunoprecipitation assay (RIPA) lysis buffer (20 mM Tris [pH 7.5], 150 mM NaCl, 1%Triton X-100, 0.1 mM EDTA supplemented with 2 μg/ml pepstatin A, 5 μg/ml leupeptin, 5 μg/ml aprotinin, 1 mM phenylmethylsulfonyl fluoride [PMSF], and 1 mM Na_3VO_4) containing a protease inhibitor cocktail. Protein concentrations were determined with a Bio-Rad (Hercules, CA) protein assay kit. Equivalent amounts of total protein were boiled in SDS sample loading buffer for 10 min and subjected to 12% SDS-PAGE. After separation, proteins were transferred to polyvinylidene difluoride membranes (Whatman, Inc.). The membranes were blocked with 3% nonfat dry milk in PBST (PBS containing 0.1% Tween 20) at room temperature for 2 h. To detect ORF020R and β-tubulin proteins, the membranes were incubated with antibodies (1:2,000 dilutions in PBST) against these proteins for 2 h at room temperature. The membranes were washed four times with PBST (each wash for 10 min), and goat anti-rabbit IgG conjugated with alkaline phosphatase or goat anti-mouse IgG conjugated with alkaline phosphatase (1:5,000 dilutions in PBST) was added as the secondary antibody. The color reaction was developed by using a nitroblue tetrazolium–5-bromo-4-chloro-3-indolylphosphate (NBT/BCIP) substrate solution.

Immunofluorescence staining. Cells were washed twice with PBS and fixed with cold methanol (−20°C) for 10 min. After three PBS rinses, the cells were permeabilized by incubation with PBS containing 0.1% Triton X-100 for 10 min and blocked with PBS containing 10% fetal calf serum (FCS). For immunostaining, cells were incubated with mouse polyclonal antiserum against ORF020R (1:200 dilutions in PBS containing 1% bovine serum albumin [BSA]) for 2 h at 37°C. Cells were washed with PBS and incubated with Alexa Fluor 488 goat anti-mouse IgG (1:300 dilutions in PBS containing 1% BSA) as the secondary antibody for 1 h and then washed three times with PBS. After staining with Hoechst 33342 for 1 min, the cells were visualized by microscopy.

Inhibition of TFV infection. HepG2 cells were plated on 48- or 6-well plates and grown to approximately 80% confluence at 27°C in a CO_2 incubator. Cells were either untreated or pretreated for 2 h at 27°C with various concentrations of the following endocytotic drugs: CPZ, chloroquine, CytoB, Baf.A1, NH_4Cl, dynasore, genistein, MβCD, okadaic acid, or nystatin. After treatment, the cells were infected with TFV, as described above, for 4 h at 27°C in the presence of the drugs. Noninternalized viruses were removed by removing virus inocula and washing the cells with citrate buffer (40 mM sodium citrate, 10 mM KCl, 135 mM NaCl [pH 3.0]) for 1 min at room temperature (27). Western blot and immunofluorescence staining analysis for ORF020R expression were carried out at 72 h postinfection.

Estimation of cellular cholesterol. Cells were incubated with 1, 5, and 10 mM MβCD for 6 h and then were scraped and homogenized with RIPA lysis buffer containing a protease inhibitor cocktail. Cholesterol levels were measured with an Amplex Red cholesterol assay kit (Molecular Probes, Eugene, OR) according to the manufacturer's instructions.

Cholesterol replenishment of MβCD-treated cells. Cells plated as described above were pretreated for 2 h at 27°C with different concentrations of cholesterol in the presence of 5 mM MβCD. Cells were then infected with TFV for 4 h at 27°C in the presence of the added compounds. After being washed with citrate buffer and PBS, cells were grown for 72 h at 27°C and then analyzed by immunofluorescence staining.

Plasmids and transfection. The dominant-negative, GFP-tagged plasmid construct pEΔ95/295 (Eps15mut), which encodes an Eps15 deletion mutant lacking the second and third EH domains but which retains binding to the adaptor complex 2, and the control plasmid pD3Δ2 that expresses a C-terminally truncated fragment of Eps15 (Eps15 control), were kindly provided by A. Benmerah, INSERM, Paris, France (3). HepG2 cells were transfected with either the GFP-tagged plasmid construct pEΔ95/295 (a dominant-negative mutant of Eps15) or negative control GFP-tagged plasmids of pD3Δ2 (D3Δ2, an Eps15 irrelevant mutant) and pEGFP-C3. Transfections were performed with Lipofectamine 2000 (Invitrogen, CA) according to the manufacturer's protocols. Transfections were typically allowed to progress for 24 h prior to infection with virus for 72 h at 27°C.

Internalization and colocalization of CTxB-AF555 with TFV. HepG2 cells were plated on coverslips the day prior to the experiment. After serum starvation

for 30 min, cells were incubated with 50 μg/ml CTxB-AF555 and TFV (MOI of 10) for 4 h and then were washed three times in PBS and fixed in cold methanol (−20°C) for 10 min. Cells were analyzed by immunofluorescence staining using mouse polyclonal antiserum against ORF020R and Alexa Fluor 488-labeled goat anti-mouse IgG.

Uptake assay. Transferrin or CTxB uptake assays were performed using Alexa 555-labeled human transferrin or CTxB. Cells were subjected to transfection with Eps15 vectors or pretreated with inhibitors. The cells incubated with 50 μg of Tf-AF555 or CTxB-AF555 for 30 min at 4°C for binding, washed, and transferred to 27°C for 30 min. Cells were washed with PBS to remove any noninternalized Tf-AF555 or CTxB-AF555 and then observed under the microscope.

RESULTS

TFV infection in HepG2 cells. To investigate if TFV is able to infect HepG2 cells, RT-PCR was used to detect transcript for the membrane protein ORF020R of TFV, and ORF020R protein was detected by Western blotting and immunofluorescence analysis. The transcripts of the ORF020R and *mcp* genes were detected in the cells infected with TFV at 72 h postinfection (Fig. 1A, lane 2) but were not detected in the control cells grown without virus (Fig. 1A, lane 1). As an internal reference, the expression of 18S rRNA was determined for both the TFV-infected and control cells (Fig. 1A). The Western blot results obtained with mouse polyclonal antiserum against ORF020R showed that the membrane protein ORF020R was present in the infected cells but not in the control cells (Fig. 1B). In contrast, β-tubulin, the internal control for Western blot analysis, was detected in both the infected and control cells (Fig. 1B). The immunostaining results also showed expression of ORF020R (green fluorescence) in HepG2 cells (Fig. 1C). Together, these data suggested that TFV was able to infect HepG2 cells, and this infection model could be used for study of TFV entry.

In this study, inhibitors that specifically block different entry pathways were used to investigate the early steps of TFV infection in HepG2 cells, including CPZ, chloroquine, CytoB, Baf.A1, NH_4Cl, caveolin-1 peptide, dynasore, genistein, MβCD, nystatin, and so on. Therefore, the cell viability and toxicological tests of most inhibitors were determined by using the CCK-8 kit. The results showed that the absorbance of inhibitors NH_4Cl (100 mM), MβCD (10 mM), nystatin (500 μg/ml), chloroquine (100 μM), genistein (200 μM), and CytoB (250 μM) had no significant difference from that of the control (Fig. 1D). Those observations suggested that the inhibitors under the above concentrations did not exhibit cytotoxic activity for HepG2 cells.

Role of clathrin-mediated endocytosis in TFV entry. Ultrastructural analysis of FV3 internalization into cells revealed a pH-dependent receptor-mediated entry pathway for viral particles that involved acidification of the endosomal and lysosomal compartments (6). To determine if TFV enters HepG2 cells through clathrin-mediated endocytosis, we treated cells with drugs that are known to inhibit this type of endocytosis and then infected the drug-treated cells with TFV virus. We first assessed the role of low pH in TFV entry by using lysosomotropic agents to disrupt the acidification of intracellular organelles. These agents, NH_4Cl and CQ, are weakly basic amines that, in their neutral forms, selectively enter cellular compartments with low internal pH and cause elevation of the pH in the target organelle. Baf.A1 which is a macrolide antibiotic that acts by inhibiting the vacuolar H^+-ATPase was employed in our study. HepG2 cells were incubated for 2 h with different concentrations of NH_4Cl, CQ, or Baf.A1 or with the control medium and then infected with TFV in the presence of these compounds for 4 h at 27°C. Infections were scored by measuring expression of the membrane protein ORF020R by immunofluorescence staining. The results showed that treatment with 1, 5, 25, 50, and 100 mM NH_4Cl significantly inhibited TFV infection by 30, 45, 65, 80, and 95%, respectively, compared to that in the untreated control (0 mM)

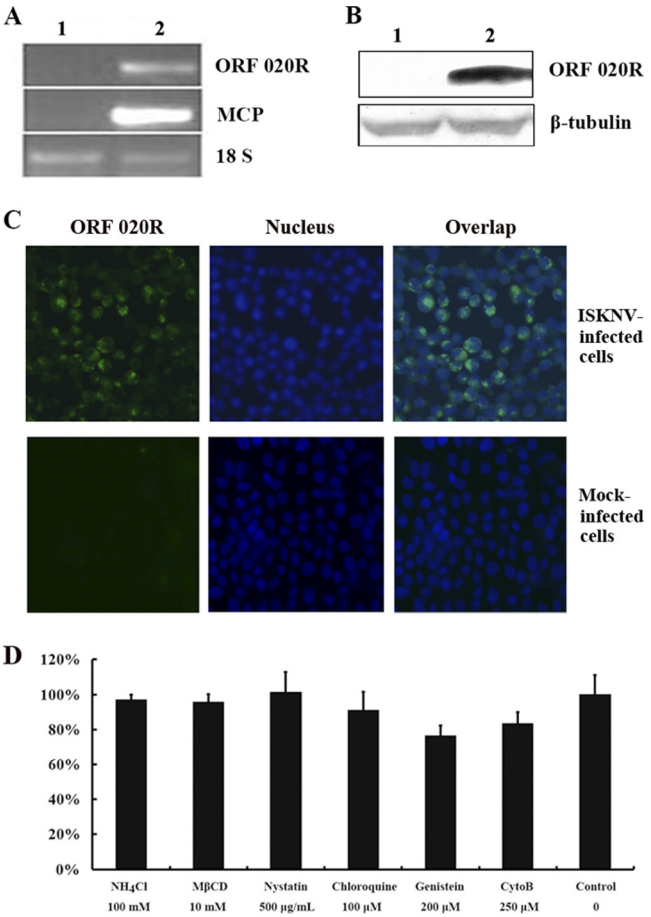

FIG. 1. RT-PCR and Western blot analysis of ORF020R. (A) RT-PCR analysis of transcription of viral genes (coding for MCP and ORF020R) in HepG2 cells after 48 h of infection with TFV. Lane 1, uninfected cells; lane 2, cells infected with TFV. 18S RNA (18 S) was used as a positive control. (B) The viral protein ORF020R was detected by Western blot analysis. Lane 1, uninfected cells; lane 2, cells infected with TFV. β-Tubulin protein was used as a positive control. (C) Detection of ORF020R expression in infectious spleen and kidney necrosis virus (ISKNV)-infected or mock-infected HepG2 cells by immunostaining. ORF020R (green fluorescence) was detected, and the nucleus was stained with Hoechst 33342 (blue fluorescence). Magnification, ×100. (D) Cell viability. HepG2 cells were plated on 96-well plates and grown to approximately 80% confluence at 27°C in a CO_2 incubator. Cells were either untreated (as a control) or treated for 6 h at 27°C with the following endocytosis inhibitors: NH_4Cl (100 mM), MβCD (10 mM), nystatin (500 μg/ml), chloroquine (100 μM), genistein (200 μM), and CytoB (250 μM). After treatment, the cells were incubated with 10 μl CCK-8 solution for 2 h, and then the cell viability was determined by the optical density at 450 nm. Data are representative of three independent experiments performed in triplicate (means ± standard error).

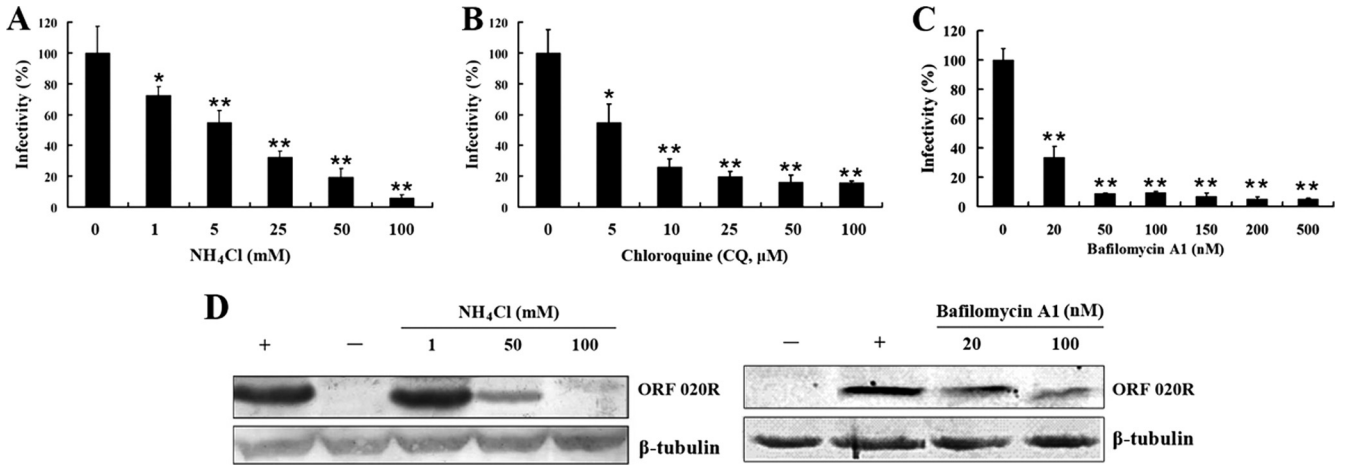

FIG. 2. Effect of alkalinization of intracellular organelles by NH_4Cl, CQ, or Baf.A1 on TFV infection. (A) Effect of NH_4Cl on TFV infection. Cells were pretreated for 2 h with various concentrations of NH_4Cl, as indicated, or without treatment (0 mM, as a positive control), and then TFV was added, and the cells were incubated for 4 h. After 72 h of incubation, cells were fixed and processed for immunofluorescence staining with mouse polyclonal antiserum against ORF020R. Viral infections were quantified as the percentage of positive treated cells relative to the number of untreated control cells. The viral infectivity of the positive control was arbitrarily set as 100%. The data shown are the means and standard deviations of the results from independent experiments. *, $P < 0.05$; **, $P < 0.01$. (B) Effect of CQ on TFV infection by immunofluorescence staining analysis. (C) Effect of Baf.A1 on TFV infection by immunofluorescence staining analysis. (D) Effects of NH_4Cl or Baf.A1 on TFV infection by Western blot analysis. Cells were treated with NH_4Cl or Baf.A1 as described above. After 72 h of incubation, cells were lysed and processed for Western blot analysis of ORF020R protein with mouse polyclonal serum. Endogenous β-tubulin was included as an internal loading control for the Western blots. +, control cells untreated with NH_4Cl; −, negative controls without TFV infection. The concentrations of NH_4Cl or Baf.A1 are indicated.

(Fig. 2A ($P < 0.05$ or $P < 0.01$). At concentrations higher than 1 mM, NH_4Cl significantly inhibited TFV entry into cells, and the inhibition was dose dependent (Fig. 2A). Similar inhibition effects were also observed with cells treated with CQ. Treatment with 5 to ~100 μM CQ significantly suppressed TFV infection by 45 to ~85% (Fig. 2B) ($P < 0.05$ or $P < 0.01$), and 20 to ~500 nM Baf.A1 also significantly inhibited TFV infection by 65 to ~95% (Fig. 2C) ($P < 0.01$), compared to that in the untreated controls (0 mM). Western blots of NH_4Cl-treated, TFV-infected cells showed that expression of ORF020R was significantly inhibited by 50 mM NH_4Cl and was almost undetectable when cells were treated with 100 mM NH_4Cl. Similarly, ORF020R expression was also significantly impaired in the cells treated with 100 nM Baf.A1 (Fig. 2D). Endogenous β-tubulin levels, included as an internal loading control for the Western blots, were unaffected by NH_4Cl or Baf.A1 treatments. Thus, TFV entry into HepG2 cells was sensitive to elevated pH and required trafficking through acidic organelles, such as early endosomes, late endosomes, lysosomes, or the *trans*-Golgi network (pH 6.0 to ~6.7).

The role of the clathrin-mediated endocytosis pathway in TFV entry was further explored using CPZ and Eps15 mutants, in which the budding of clathrin-coated pits (CCPs) is disturbed. CPZ has been used extensively to inhibit clathrin-mediated uptake of viruses and is known to cause the clathrin lattice to assemble on endosomal membranes, and at the same time prevents the assembly of coated pits at the plasma membrane by controlling AP-2 binding to membranes (58). To test the efficacy of the CPZ in clathrin endocytosis, cells were subjected to 10 μM CPZ treatment and then a transferrin uptake assay was performed. Our results showed that cells untreated with CPZ allowed normal transferrin uptake, whereas cells treated with 10 μM CPZ were blocked in the uptake of transferrin (Fig. 3D). The effect of CPZ on TFV internalization by cells was first assessed by immunofluorescence staining. Unexpectedly, no obviously inhibition of TFV infection was observed when cells were treated with 5 to ~250 μM CPZ (Fig. 3A): no inhibition of expression of ORF020R was observed in the cells treated with 100 and 200 μM CPZ compared to the level in the untreated control cells (Fig. 3B). Those results suggested that the mechanism of TFV entry might be different from transferrin and was independent of the CCPs' budding.

Further confirmation that TFV entry is independent of CCPs budding was obtained by expressing a dominant-negative Eps15 protein in the cells. Eps15 is found at the growing edges of clathrin-coated pits and participates in the formation of budding coated vesicles (60). Overexpression of an Eps15 mutant protein (EΔ95/295) lacking the second and third EH domains results in the inhibition of CCP assembly (3). To test the efficacy of the Eps15 plasmid in our system, we transiently transfected HepG2 cells, using enhanced GFP (EGFP) alone as a positive control, and then performed a transferrin uptake assay. It has been reported previously that expression of EΔ95/295 prevents transferrin internalization (53). Our results agreed with this finding, since cells transfected with EGFP allowed normal transferrin uptake, whereas cells expressing EΔ95/295 were unable to internalize the transferrin (Fig. 3E). However, the Western blotting results showed that the protein level of ORF020R in the cells transfected with pEΔ95/295 did not change compared to those transfected with negative controls pD3Δ2 (an Eps15 irrelevant mutant) and pEGFP-C3 (Fig. 3C). Endogenous β-tubulin was included as an internal

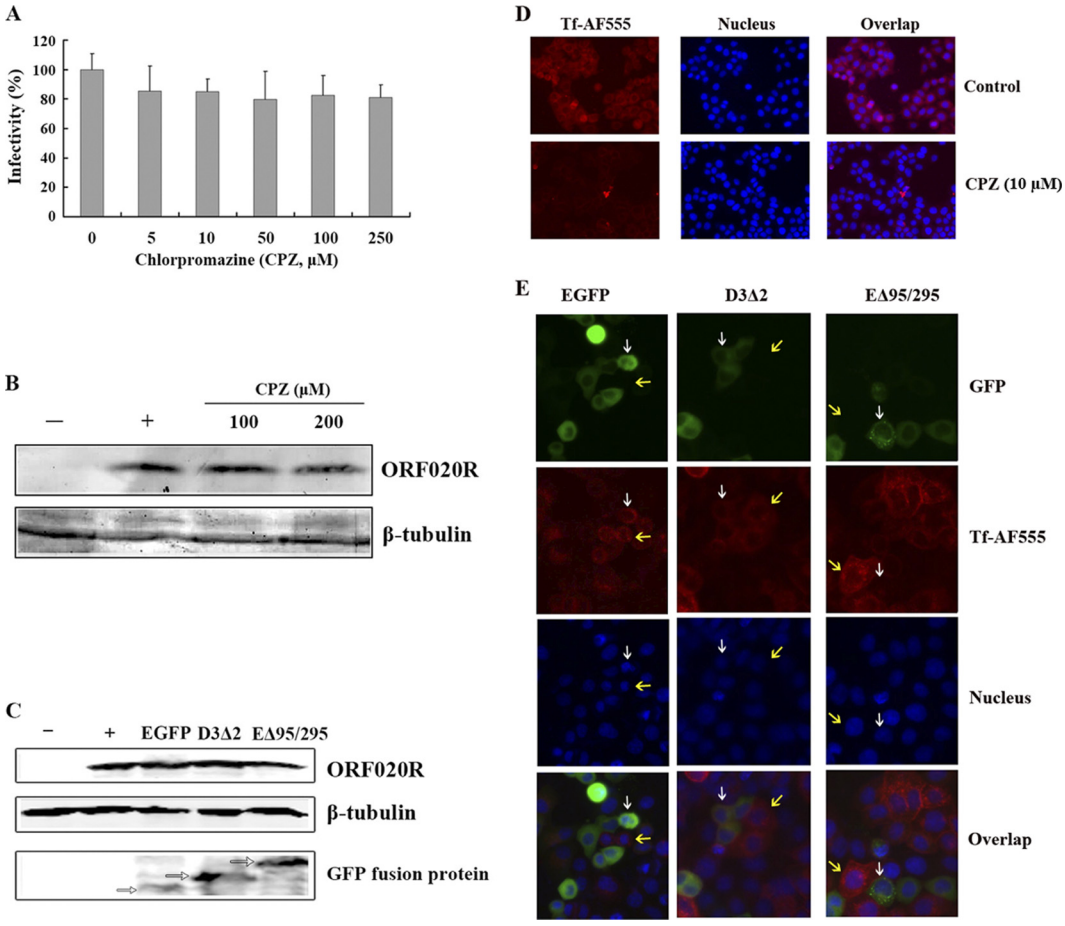

FIG. 3. Effects of CPZ and Eps15 on TFV infection. (A) Effect of CPZ on TFV infection measured by immunofluorescence staining analysis. Cells were pretreated for 2 h with various concentrations of CPZ, as indicated, or without treatment (0 mM, as a positive control), and then TFV was added, and the cells were incubated for 4 h. After 72 h of incubation, the cells were fixed and processed for immunofluorescence staining with mouse polyclonal antiserum against ORF020R. Viral infections were quantified as the percentage of positive, treated cells relative to the number of untreated control cells. The viral infectivity of cells untreated with reagents (as a positive control) was arbitrarily set as 100%. The data shown are the means and standard deviations of the results from independent experiments. (B) Effect of CPZ on TFV infection by Western blot analysis. Cells were treated with CPZ as described above. After 72 h of incubation, cells were lysed and processed for Western blot analysis of ORF020R protein with mouse polyclonal serum. Endogenous β-tubulin was included as an internal loading control for the Western blots. −, negative controls without TFV infection; +, control cells untreated with CPZ. The concentrations of 100 and 200 μM CPZ are indicated. (C) Effect of dominant-negative Eps15 protein on TFV infection by Western blot analysis. Cells were transfected with either the GFP-tagged plasmid construct pEΔ95/295 (a dominant-negative mutant of Eps15) or negative control GFP-tagged plasmids of pD3Δ2 with an Eps15 irrelevant mutant (D3Δ2) and pEGFP-C3, and then the entry of TFV was measured as the level of ORF020R protein by Western blot analysis. Endogenous β-tubulin was included as an internal loading control, and the GFP fusion proteins (white arrows) were detected with rabbit polyclonal anti-GFP antibody for the Western blot analysis. −, negative controls without TFV infection; +, control cells not transfected with plasmids. (D) Cells were either untreated (as a positive control) or pretreated with 10 μM CPZ for 2 h at 27°C and washed with PBS. Cells were incubated with 10 μM CPZ containing 50 μg AF555-Tf for 30 min at 4°C for binding, washed, and then transferred to 27°C for 30 min. Cells were washed with PBS to remove any uninternalized AF555-Tf and then observed under the microscope. Magnification, ×100. (E) Cells were transiently transfected with either pEΔ95/295, pD3Δ2, or pEGFP vector. After 24 h posttransfection, the cells were incubated with 50 μg of Tf-AF555 for 30 min at 4°C for binding, washed, and transferred to 27°C for 30 min. Cells were washed with PBS to remove any noninternalized Tf-AF555 and then fixed for viewing. White arrows indicate that cells expressed the EGFP fusion proteins; yellow arrows indicate that cells did not express the EGFP fusion proteins. Magnification, ×100.

loading control, and the GFP fusion recombinant proteins were detected by anti-GFP antibodies.

Role of caveola-dependent endocytosis in TFV entry. Next, to evaluate if TFV internalization occurs via the caveola-mediated endocytosis pathway, drugs that selectively inhibit this pathway were applied at the early stage of TFV entry. Cholesterol is a prominent component of lipid rafts and is required for caveola formation. Depletion of cholesterol from the membranes with MβCD or sequestration of cholesterol with nystatin has been shown to impair caveola-mediated endocytosis (52). The effects of MβCD or nystatin on TFV internalization into cells were determined by immunofluorescence staining. As shown in Fig. 4A, treatment of the cells with 2, 5, and 10 mM MβCD inhibited TFV infection by 55, 80, and 98%, respectively, compared to the untreated control (0 mM), while no inhibition was observed for MβCD concentrations of 0.5 and 1 mM. Nystatin showed a similar inhibitory effect on TFV entry (Fig. 4B), where treatment of cells with 100 and 500 μg/ml

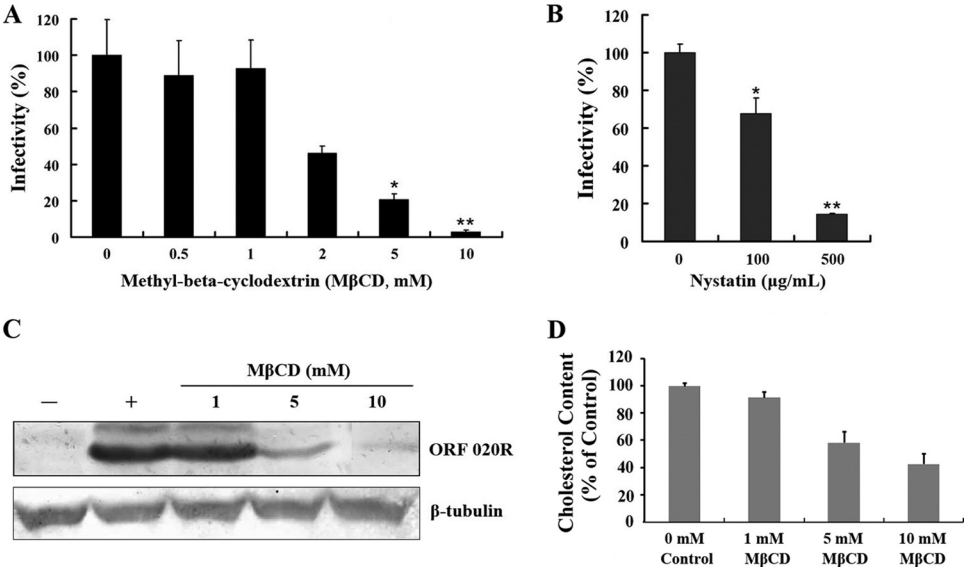

FIG. 4. Effects of MβCD and nystatin on TFV infection. (A) Effect of cholesterol depletion by MβCD on TFV infection as determined by immunofluorescence staining analysis. Cells were pretreated for 2 h with various concentrations of MβCD, as indicated, or were untreated (0 mM, as a positive control), and then TFV was added, and the cells were incubated for 4 h. After 72 h of incubation, cells were fixed and processed for immunofluorescence staining with mouse polyclonal antiserum against ORF020R. Viral infections were quantified as the percentage of positive, treated cells relative to the number of untreated control cells. The viral infectivity of cells untreated with reagents (as positive control) was arbitrarily set as 100%. The data shown are the means and standard deviations of the results from independent experiments. *, $P < 0.05$; **, $P < 0.01$. (B) Effect of cholesterol sequestration by nystatin on TFV infection as measured by immunofluorescence staining. (C) Effect of MβCD on TFV infection as measured by Western blot analysis. Cells were treated with MβCD as described above. After 72 h of incubation, cells were lysed and processed for Western blot analysis of ORF020R protein with mouse polyclonal serum. Endogenous β-tubulin was included as an internal loading control. +, control cells untreated with MβCD; −, negative controls without TFV infection. The concentrations of 1, 5, and 10 mM MβCD are indicated. (D) Total cellular cholesterol. Cells were incubated with 1, 5, and 10 mM MβCD for 6 h and then were scraped and homogenized with RIPA lysis buffer containing a protease inhibitor cocktail. Cholesterol levels were measured with an Amplex Red cholesterol assay kit (Molecular Probes, Eugene, OR) according to the manufacturer's instructions. The data shown are the means ± standard errors of triplicate points from two independent experiments.

nystatin significantly inhibited TFV entry by 32% ($P < 0.05$) and 86% ($P < 0.01$), respectively. Western blot results also showed an inhibitory effect of MβCD on ORF020R expression. As shown in Fig. 4C, 1 mM MβCD did not significantly change the level of ORF020R protein; however, ORF020R expression was significantly inhibited by concentrations of MβCD 5 mM or higher. To illustrate that the levels of cellular cholesterol were depleted by MβCD, the amounts of the cellular cholesterol were quantified with the Amplex Red cholesterol assay kit according to the manufacturer's instructions. The results showed that depletion of cholesterol from the membranes resulted in ~40% and 60% reduction of total cellular cholesterol when 5 and 10 mM MβCD was used, whereas the level of cellular cholesterol was not significant reduced when cells were treated with 1 mM MβCD (Fig. 4D). Those observations suggested that the TFV entry was associated with the levels of the cells' membrane cholesterol.

The role of membrane cholesterol in virus uptake was further clarified by cholesterol replenishment experiments. Cells were pretreated with cholesterol and then treated with or without MβCD for 2 h at 27°C prior to TFV infection. As shown in Fig. 5, pretreatment of cells with 5 μg/ml (C), 25 μg/ml (E), or 50 μg/ml (G) cholesterol alone did not have any effect on TFV infection, compared to that in the untreated control (Fig. 5A). However, TFV infection was significantly inhibited in the cells treated with 5 mM MβCD alone (Fig. 5B), as described above. This inhibition of TFV infection by MβCD was prevented in the cells pretreated with 5 μg/ml (D), 25 μg/ml (F), or 50 μg/ml (H) cholesterol, and the response was dose dependent. Thus, TFV internalization into cells depended on membrane cholesterol, suggesting involvement of the caveola-mediated endocytosis pathway.

Since caveolar budding is regulated by reversible phoshorylation (39), the effects of genistein and okadaic acids on TFV infection were also determined. Cells were pretreated with genistein, a tyrosine kinase inhibitor known to disrupt caveola-related endocytosis (51), prior to TFV infection, and the virus entry was evaluated at 72 h postinfection. As shown in Fig. 6A, treatment of cells with 10, 20, 50, and 100 μM genistein inhibited TFV infection by ~17, 26, 37, and 51%, respectively ($P < 0.05$), and treatment with 200 μM genistein inhibited TFV infection by 55% ($P < 0.05$), compared to that of the untreated control (0 mM). Cells were also pretreated with okadaic acid, an inhibitor of phosphatase 1 and 2A that is known to stimulate caveola-mediated entry and to inhibit the clathrin-mediated endocytic pathway (62), to determine the effect of caveolar budding on the TFV infection. As shown in Fig. 6B, treatments with 0.05 and 0.1 μM okadaic acid had no effect on TFV infection, while TFV infection was significantly increased with treatments of 0.25 to ~1 μM okadaic acid ($P < 0.05$). Thus, TFV entry appeared to involve the caveola-mediated rather than clathrin-mediated endocytic pathway.

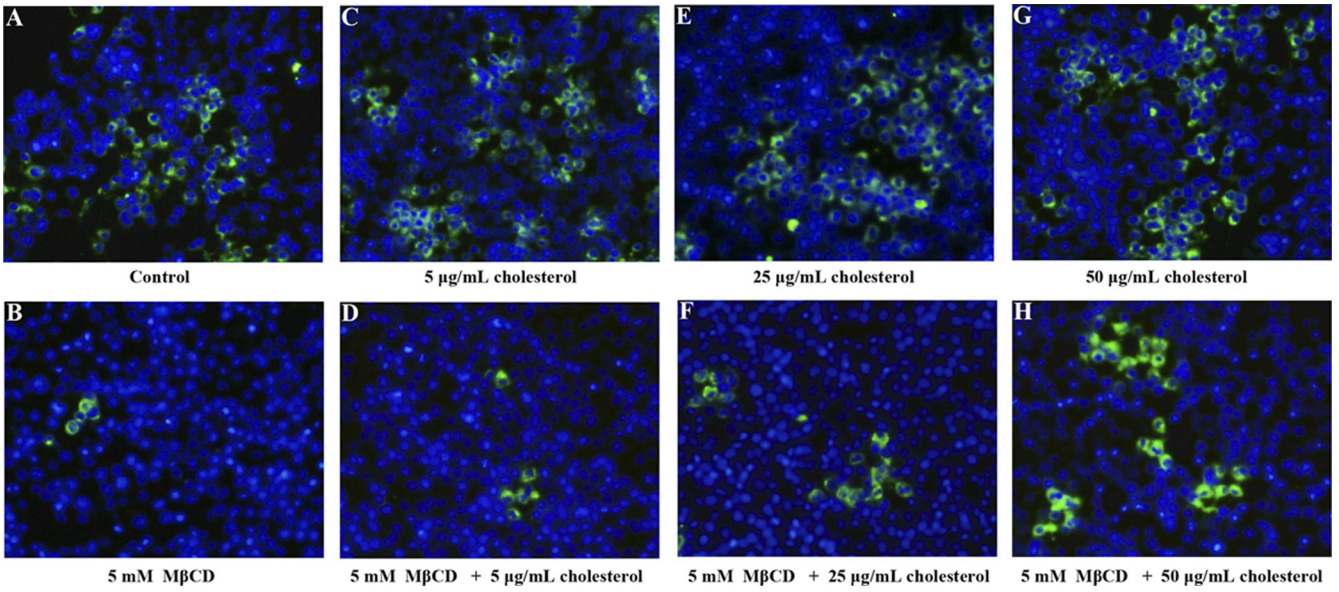

FIG. 5. Effect of cholesterol replenishment in MβCD-treated cells on TFV infection as measured by immunofluorescence analysis. Cell monolayers were pretreated with cholesterol with or without MβCD for 2 h, and then TFV was added and the mixture was incubated for 4 h. After 72 h of incubation, cells were fixed and processed for immunofluorescence staining with mouse polyclonal antiserum against ORF020R. Nuclei (blue) were visualized with Hoechst 33342. Cells were treated with 0 μg/ml cholesterol (control) (A), 5 mM MβCD (B), 5 μg/ml cholesterol (C), 5 mM MβCD and 5 μg/ml cholesterol (D), 25 μg/ml cholesterol (E), 5 mM MβCD and 25 μg/ml cholesterol (F), 50 μg/ml cholesterol (G), or 5 mM MβCD and 50 μg/ml cholesterol (H). Magnification, ×100.

The role of caveolin-1 protein in TFV infection was also assessed. Previous studies have shown that overexpression of caveolin-1 could negatively regulate caveolar budding in mammalian cells (30). Cells were treated with different concentrations of the caveolin-1 peptide or control peptide prior to TFV infection, and TFV internalization was then evaluated by Western blotting. As shown in Fig. 6C, the protein levels of ORF020R were reduced when cells were treated with 1, 2, and 5 μM caveolin-1 peptide, compared to the level of the untreated control (0 μM), and the inhibition was dose dependent. The ORF020R protein was barely detectable in cells treated with 5 μM caveolin-1 peptide, whereas the protein levels of ORF020R were not significant reduced when cells were treated with 1, 2, and 5 μM control peptide. Thus, TFV entry appeared to occur via caveolar budding and could be inhibited by an overdose of caveolin-1 peptide.

CTxB binds to endogenous GM1 and is internalized by the caveolar endocytotic pathway. It is then delivered to the Golgi complex, which results in a characteristic formation of a nuclear ring pattern characteristic of the endoplasmic reticulum (ER) (36). To demonstrate that the caveolin-l peptide inhibition of TFV entry was associated with caveola endocytosis, the caveolin-1 peptide was employed to analyze the uptake of transferrin and CTxB. As shown in Fig. 7A, normal transferrin uptake occurred in untreated cells or in cells treated with caveolin-l peptide. However, untreated cells allowed normal CTxB uptake, whereas cells treated with 5 μm caveolin-l peptide were impaired in internalization of CTxB. The role of caveola-mediated endocytosis was further explored by immunofluorescence colocalization. Cells were incubated with TFV and CTxB-AF555 for 4 h at 27°C and then immunostained with mouse polyclonal antiserum against ORF020R. As shown in Fig. 7, both TFV (A; green fluorescence) and CTxB-AF555 (B; red fluorescence) formed nuclear ring patterns, and an overlay of the red and green channels showed that some TFV particles colocalized with CTxB-AF555 (C). This result indicated that TFV entry paralleled that of CTxB and appeared to occur via caveolae.

Roles of dynamin and actin in TFV entry. Dynamin is a GTPase that seems to be a master regulator of membrane trafficking events occurring at the cell surface (38). Dynamin is essential for clathrin-coated vesicle formation and transport, as well as for ligand uptake through caveola-mediated endocytosis (20), and is required for the uptake of several viruses (21). A small molecule called dynasore, which rapidly inhibits the GTPase activity of dynamin with high specificity (1), was used to determine whether dynamin is involved in TFV entry. The immunofluorescence results showed that treatment of the cells with 50, 100, and 200 μM dynasore inhibited TFV infection by 45% ($P < 0.05$), 55% ($P < 0.01$), and 71% ($P < 0.01$), respectively, compared to that in the untreated control (0 mM), while no marked inhibition was observed for doses lower than 20 μM (Fig. 8A). Western blotting also confirmed that level of ORF020R was reduced when cells were treated with 100 μM dynasore, and ORF020R could only be weakly detected when cells were treated with 200 μM dynasore (Fig. 8A). Thus, TFV entry appeared to use a dynamin-dependent endocytosis pathway.

To study the cytoskeleton effect on TFV entry, an actin polymerization inhibitor, CytoB, was used. The immunostaining results shown in Fig. 8B indicate that treatment of cells with 5 to ~250 μM CytoB significant inhibited TFV infections by 40 to ~50% ($P < 0.05$ or $P < 0.01$). The protein levels of

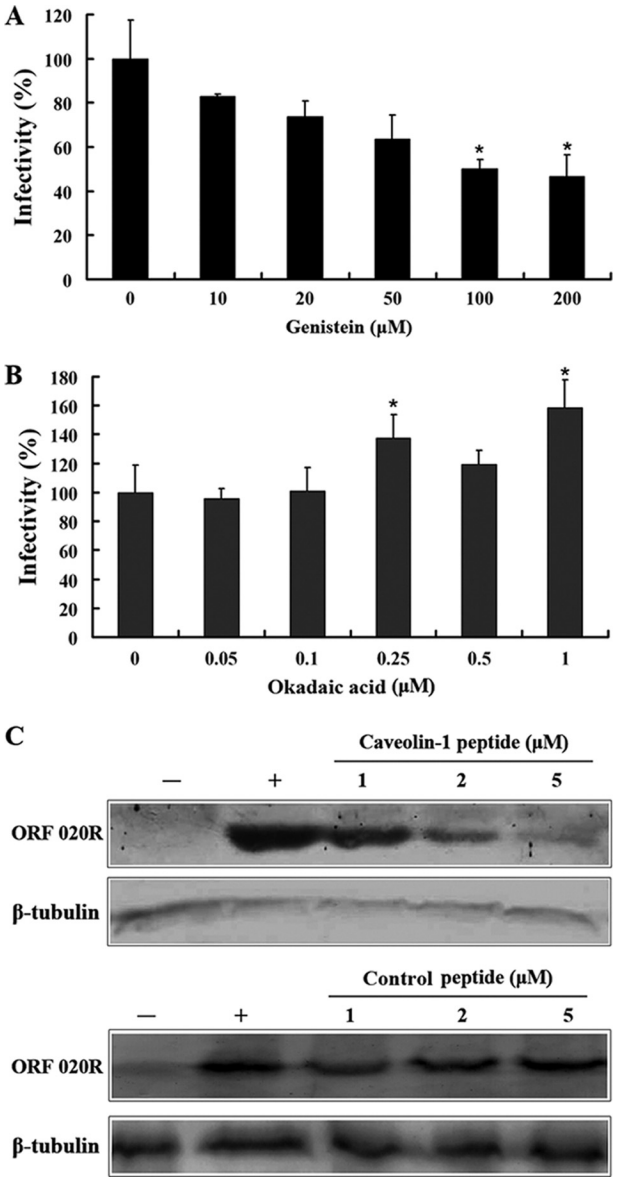

FIG. 6. Effects of genistein, okadaic acid, and caveolin-1 peptide on TFV infection. (A) Genistein effect on TFV infection as measured by immunofluorescence staining analysis. Cells were pretreated for 2 h with various concentrations of genistein, as indicated, or without treatment (0 mM, as a positive control), and then TFV was added and the cells were incubated incubated for 4 h. After 72 h of incubation, cells were fixed and processed for immunofluorescence staining with mouse polyclonal antiserum against ORF020R. Viral infections were quantified as the percentage of positive, treated cells relative to the number of untreated control cells. The viral infectivity of cells untreated with reagents (as positive control) was arbitrarily set as 100%. The data shown are the means and standard deviations of the results from independent experiments. *, $P < 0.05$. (B) Effect of okadaic acid on TFV infection as measured by immunofluorescence staining analysis. (C) Effect of caveolin-1 scaffolding domain peptide (caveolin-1 peptide) on TFV infection by Western blot analysis. Cells were treated with caveolin-1 peptide or control peptide as described above. After 72 h of incubation, cells were lysed and processed for Western blot analysis of ORF020R protein with mouse polyclonal serum. Endogenous β-tubulin was included as an internal loading control for the Western blot. +, control cells untreated with MβCD; −, negative controls without TFV infection. The 1, 2, and 5 μM concentrations of caveolin-1 peptides are indicated.

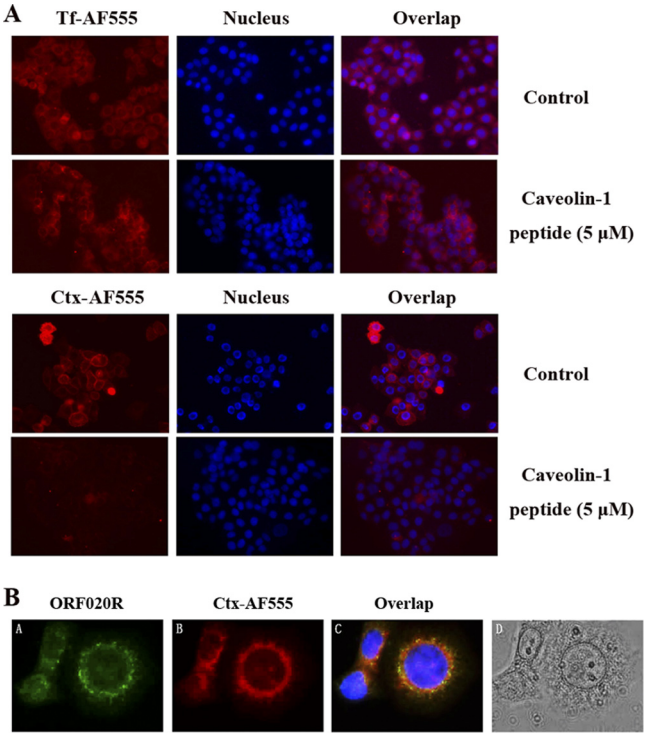

FIG. 7. Immunofluorescence staining analysis. (A) Effects of caveolin-1 peptide on transferrin and CTxB uptake. Cells were untreated (as a positive control) or pretreated with 5 μM caveolin-1 peptide for 2 h at 27°C and washed with PBS. The cells were incubated with 5 μM caveolin-1 peptide containing 50 μg of AF555-CtxB or AF555-Tf for 30 min at 4°C for binding, washed, and transferred to 27°C for 30 min. Cells were washed with PBS to remove any uninternalized AF555-CtxB or AF555-Tf and then observed under the microscope. Magnification, ×100. (B) Immunofluorescence staining analysis of TFV and CTxB internalization. (B, panel A) TFV particles were stained with 020R antibody as the primary antibody and Alexa Fluor 488-labeled goat anti-mouse IgG (green) as the secondary antibody. (B, panel B) CTxB was conjugated with Alexa Fluor 555-conjugated (red). (B, panel C) Nuclei (blue) were visualized with Hoechst 33342. (B, panel D) Phase-contrast imaging. Magnification, ×400.

ORF020R were also decreased when cells were treated with 100 to ~200 μM CytoB, as revealed by Western blots (Fig. 8B). These results were consistent with previous reports showing that caveolar endocytosis was ligand triggered and involved extensive rearrangement of the actin-associated cytoskeleton (46).

DISCUSSION

As obligate intracellular parasites, all viruses must have ways of entering target cells to initiate replication and infection. Viruses are now known to have evolved many versions of endocytosis to effect entry into host cells, including clathrin-mediated endocytosis, caveola-mediated endocytosis, and macropinocytosis (11, 65). Within a virus family, different members may employ different endocytosis pathways. For example, in the polyomaviruses, the JC virus (JCV) enters host cells by pH-dependent clathrin-mediated endocytosis (49), simian virus 40 (SV40) enters host cells by a pH-independent endocytosis via caveolae (46), and the BK virus (BKV) is internalized

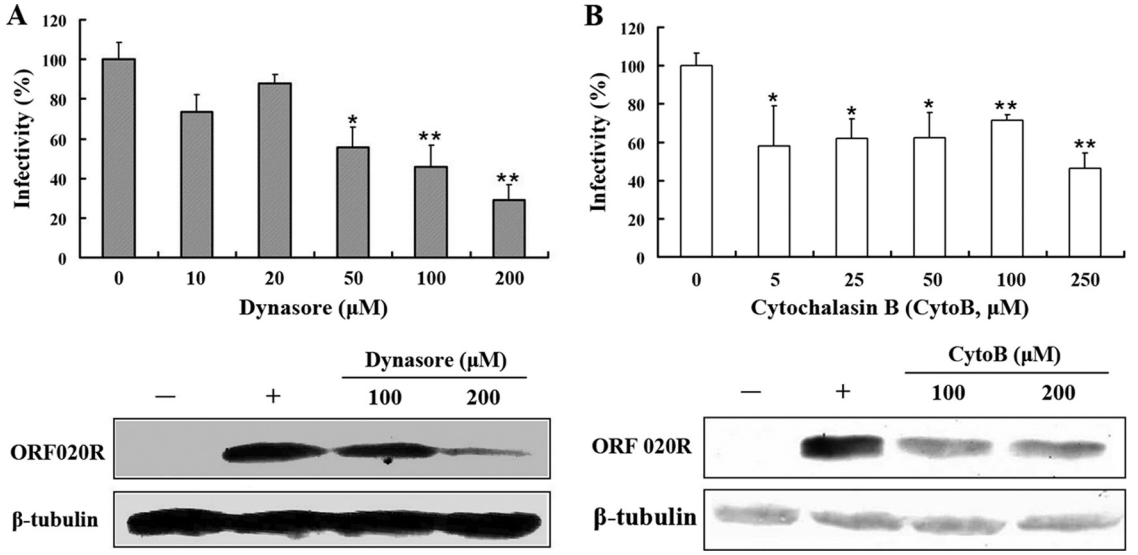

FIG. 8. Effects of dynamin and the actin cytoskeleton on TFV infection. (A) Effect of dynasore inhibition of dynamin on TFV infection. (B) Effect of CytoB inhibition of actin polymerization on TFV infection. Cells were pretreated for 2 h with various concentrations of dynasore or CytoB, as indicated, or were not treated (0 mM, as a positive control), and then TFV was added, and the cells were incubated for 4 h. After 72 h of incubation, cells were processed for immunofluorescence staining or Western blot analysis with mouse polyclonal antiserum against ORF020R. For immunofluorescence staining, viral infections were quantified as the percentage of positive treated cells relative to the number of untreated control cells. The viral infectivity of cells untreated with reagents (as positive control) was arbitrarily set as 100%. The data shown are the means and standard deviations of the results from independent experiments. *, $P < 0.05$; **, $P < 0.01$. For Western blotting, endogenous β-tubulin was included as an internal loading control. +, control cells untreated with drugs; −, negative controls without TFV infection. The concentrations of drugs are indicated.

by a pH-dependent caveola-mediated endocytosis pathway (12), while still other polyomaviruses enter host cells by using a class of uncoated vesicles in a manner that is independent of either clathrin or caveolae (13). However, little is known regarding the endocytosis pathways used by iridoviruses that infect lower vertebrates. In the early 1980s, research on FV3 entry revealed that enveloped FV3 particles were internalized into BHK cells by adsorptive endocytosis via coated pits and then appeared to move through endosomes and ultimately to lysosomes (6–8). The mechanism of FV3 entry, replication, assembly, and budding has been recognized as a model for the iridovirus life cycle (16). Currently, more than 100 iridoviruses have been isolated and researched with respect to identification of viral structural genes and functional viral proteins (15), but little is known about early events in iridovirus infection, and few studies have focused on cell entry mechanisms used by iridoviruses. Thus, whether the model of FV3 entry explains cellular entry mechanisms for all iridoviruses is not yet clear (68). In the present paper, we show that TFV entry into host cells occurs by a pH-dependent, dynamin-dependent endocytotic pathway involving caveolae.

We first examined the possibility of a clathrin-mediated pathway as an initial step in TFV entry into cells. The classic clathrin-mediated endocytosis involves CCP formation, assembly, and budding, followed by CCP transport into acidic endosomal and lysosomal compartments (33). The clathrin-mediated endocytosis pathway was considered a likely candidate for TFV entry as this is the pathway used by FV3 (14). The dose-dependent inhibition of TFV entry by NH_4Cl, CQ, or Baf.A1 (Fig. 2) suggested involvement of a low-pH organelle. However, disruption of CCP assembly and budding (3, 58) by CPZ treatment or transfection with a dominant-negative mutant Eps15 plasmid (pEΔ95/295) had no effect on TFV infection (Fig. 3). TFV was capable of entering cells lacking the capacity for CCP assembly and internalization. Thus, unlike FV3 infection of BHK cells, TFV entry did not appear to involve coated pits, which distinguishes it from other animal viruses that use a class clathrin-mediated endocytosis pathway (6). Clathrin-mediated endocytosis has been clearly demonstrated by CPZ treatment or use of Eps15 mutants for viruses such as West Nile virus (9), rubella virus (26), Junín arenavirus (33), influenza virus (53), rhinovirus (55), African swine fever virus (21), dengue virus serotype 2 (47), and the polyomavirus JC virus (49), among others. No evidence has been found for other modes of virus entry, such as caveola-mediated endocytosis or macropinocytosis, for these other viruses (44).

Since TFV entry was clearly not dependent on clathrin, this raised the question of whether there was any pH dependence. In general, pH dependence of viral infections is regarded as a hallmark of clathrin-mediated endocytosis that distinguishes it from the other endocytoses: for example, caveola-mediated endocytosis, which is considered to occur in a pH-neutral setting that bypasses the acidic endosomes (18). A nonclassical endosomal structure that tests positive for calveolin-1 has been shown to deliver caveola-internalized cargo to the Golgi complex, an organelle with an acidic pH ranging from 6.0 to 6.7, *trans* to *cis* (30, 40). Since viral uncoating is promoted by low pH (12, 67), the Golgi complex is a potential site for this process.

We therefore next evaluated the potential involvement of caveola-mediated endocytosis in TFV internalization. The inhibitory effects of the cholesterol-depleting agent MβCD and

cholesterol-sequestrating agent nystatin on TFV infection (Fig. 4), as well as the prevention of the inhibitory effects of MβCD on TFV infection by exogenously supplied cholesterol (Fig. 5), suggested the involvement of cholesterol-rich membrane subdomains such as caveolae or lipid rafts. For SV40 virus, infection of susceptible cells is also highly sensitive to disruption of caveolar function resulting from alterations in the target cells (45). Similar to our experiments with cholesterol replenishment, infection by human herpesvirus 6 (HHV-6) was abolished when cholesterol was removed by MβCD, but the inhibition could be rescued by addition of exogenous cholesterol (22).

To provide further evidence for the involvement of caveolae in the TFV entry, genistein and okadaic acid were used. Genistein, a tyrosine kinase inhibitor, strongly blocked TFV infection, while okadaic acid, an inhibitor of phosphatases 1 and 2A, was beneficial for TFV infection (Fig. 6). Similar effects have been reported for entry of other viruses or of CTxB through caveola-mediated endocytosis pathways (45, 54). In the present study, a role for caveolin-1 was implicated by using the caveolin-1 scaffolding domain peptide, which is functional equivalent of caveolin-1 protein (4). Caveolin-1 is not necessary for clathrin-independent endocytosis, as shown by caveolin-1 small interfering RNA (siRNA) experiments (62) and by the fact that cholesterol-dependent, clathrin-independent endocytosis occurs in cells that naturally lack both caveolin-1 and abundant caveola structures (29, 39, 43). Inactivation of caveolin-1 by siRNA or dominant-negative mutants might not be best for directly determining virus entry via caveolae. However, overexpression of caveolin-1 has been shown to negatively regulate the budding of caveolae (30, 35). The explanation was given that overexpression of caveolin-1 might stabilize caveolar structures at the plasma membrane, preventing caveolar budding (39). Our results showed that cell treatment with caveolin-1 peptides significantly reduced TFV infection in a dose-dependent manner (Fig. 6C), suggesting that TFV was internalized via caveolar budding. Colocalization of internalized CTxB-AF555 with TFV and the formation of nuclear ring patterns (Fig. 7B) provided further support. CTxB is known to bind to endogenous GM1 and is internalized by the caveolar endocytosis pathway, followed by delivery to the Golgi complex (36). TFV entry was consistent with uptake of CTxB via caveolae and delivery to the Golgi-ER complexes, in accordance with our previous hypothesis of TFV entry through a pH-dependent but atypical caveola-mediated endocytosis pathway.

The evidence presented here indicates that TFV entry into HepG2 cells occurs by a pH-dependent, cholesterol-dependent, and caveolin-1-sensitive endocytosis via caveolae. A similar pH-dependent atypical caveola-mediated endocytosis has also been reported for BKV entry into Vero cells. Eash et al. (12) revealed that BKV entry into permissive Vero cells is slow, independent of clathrin-coated pit assembly, dependent on an intact caveolin-1 scaffolding domain, and requires cholesterol, and the viral particles colocalize with CTxB. Entry of polyomaviruses into cells also occurs via various pathways, as described previously. With the same wide range of hosts and double-stranded DNA (dsDNA) as polymaviruses, entry of iridoviruses into cells may also involve various endocytosis pathways.

An important insight in recent years has been the recognition that trafficking between different membrane compartments involves not only classical adaptors and coat proteins but also the recruitment of actin associated with the cytoskeleton, which may participate in sorting processes (48). A recent study of TFV infection of zebrafish embryonic fibroblast (ZF4) cells showed that reorganization of the cytoskeleton contributed to TFV infection (31). In the present study, TFV entry was inhibited by the actin polymerization inhibitor CytoB (Fig. 8B), in agreement with a previous report that caveolar endocytosis is ligand triggered and involves extensive rearrangement of the actin cytoskeleton (46). SV40 particles have been reported to induce transient breakdown of actin stress fibers following binding to caveolae. Actin and dynamin are then recruited to virus-loaded caveolae as actin patches that serve as sites for actin "tail" formation. These are necessary for formation of caveola-derived endocytic vesicles and for infection of the cells.

Finally, we have detected the effect of some chemicals (random selected) on the virus attachments to cells by Western blotting. The results showed that caveolin-1 peptide (5 μM), NH_4Cl (100 mM), MβCD (5 mM), or cholesterol (50 μg/ml) was not interfering with the TFV attachment to cells (data not shown). So, we suggested that the effects of drugs were on the TFV entry, rather than on the TFV attachment to cells.

In summary, our data indicate that TFV entry into HepG2 cells is dependent on an acidic endosomal pH but does not require the assembly or invagination of CCPs. The endocytotic pathway involved in TFV entry is dependent on membrane cholesterol, inhibited by caveolin-1 scaffolding domain peptide, and colocalizes with the caveola-mediated endocytic marker CTxB. In addition, TFV entry is dependent on dynamin and actin associated with the cytoskeleton. Thus, TFV enters HepG2 cells by an atypical caveola-mediated endocytosis that involves a pH-dependent step.

ACKNOWLEDGMENTS

This work was supported by the National Natural Science Foundation of China under grants U0631008 and 31001123, the National Basic Research Program of China under grant 2006CB101802, the National High Technology Research and Development Program of China (863 Program) under grants 2006AA09Z445 and 2006AA100309, the Priming Scientific Research Foundation for the Junior Teachers in Sun Yat-Sen University, and the China Postdoctoral Science Foundation.

REFERENCES

1. **Abazeed, M. E., J. M. Blanchette, and R. S. Fuller.** 2005. Cell-free transport from the trans-golgi network to late endosome requires factors involved in formation and consumption of clathrin-coated vesicles. J. Biol. Chem. **280:** 4442–4450.
2. **Beer, C., D. S. Andersen, A. Rojek, and L. Pedersen.** 2005. Caveola-dependent endocytic entry of amphotropic murine leukemia virus. J. Virol. **79:** 10776–10787.
3. **Benmerah, A., M. Bayrou, N. Cerf-Bensussan, and A. Dautry-Varsat.** 1999. Inhibition of clathrin-coated pit assembly by an Eps15 mutant. J. Cell Sci. **112:**1303–1311.
4. **Bernatchez, P. N., et al.** 2005. Dissecting the molecular control of endothelial NO synthase by caveolin-1 using cell-permeable peptides. Proc. Natl. Acad. Sci. U. S. A. **102:**761–766.
5. **Bishop, N. E.** 1997. An update on non-clathrin-coated endocytosis. Rev. Med. Virol. **7:**199–209.
6. **Braunwald, J., H. Nonnenmacher, and F. Tripier-Darcy.** 1985. Ultrastructural and biochemical study of frog virus 3 uptake by BHK-21 cells. J. Gen. Virol. **66:**283–293.
7. **Chinchar, V. G., et al.** 2005. Family Iridoviridae virus, p. 145–162. *In* C. M. Fauquet, M. A. Mayo, J. Maniloff, U. Desselberger, and L. A. Ball (ed.), Taxonomy of virus. Elsevier/Academic Press, San Diego, CA.
8. **Chinchar, V. G., A. Hyatt, T. Miyazaki, and T. Williams.** 2009. Family

Iridoviridae: poor viral relations no longer. Curr. Top. Microbiol. Immunol. **328:**123–170.
9. **Chu, J. J., and M. L. Ng.** 2004. Infectious entry of West Nile virus occurs through a clathrin-mediated endocytic pathway. J. Virol. **78:**10543–10555.
10. **Delius, H., G. Darai, and R. M. Flügel.** 1984. DNA analysis of insect iridescent virus 6: evidence for circular permutation and terminal redundancy. J. Virol. **49:**609–614.
11. **Dimitrov, D. S.** 2004. Virus entry: molecular mechanisms and biomedical applications. Nat. Rev. Microbiol. **2:**109–122.
12. **Eash, S., W. Querbes, and W. J. Atwood.** 2004. Infection of vero cells by BK virus is dependent on caveolae. J. Virol. **78:**11583–11590.
13. **Gilbert, J. M., and T. L. Benjamin.** 2000. Early steps of polyomavirus entry into cells. J. Virol. **74:**8582–8588.
14. **Goorha, R.** 1982. Frog virus 3 DNA replication occurs in two stages. J. Virol. **43:**519–528.
15. **Goorha, R., and A. Granoff.** 1979. Icosahedral cytoplasmic deoxyriboviruses, p. 347–399. *In* H. Fraenkel-Conrat and R. R. Wagner (ed.), Comprehensive virology. Plenum, New York, NY.
16. **Goorha, R., and K. G. Murti.** 1982. The genome of frog virus 3, an animal DNA virus, is circularly permuted and terminally redundant. Proc. Natl. Acad. Sci. U. S. A. **79:**248–252.
17. **Guo, C. J., et al.** 2009. The Jak and Stat family members of the mandarin fish *Siniperca chuatsi*: molecular cloning, tissues distribution and immunobiological activity. Fish Shellfish Immunol. **27:**349–359.
18. **Hasebe, R., et al.** 2009. Infectious entry of equine herpesvirus-1 into host cells through different endocytic pathways. Virology **393:**198–209.
19. **He, J. G., et al.** 2002. Sequence analysis of the complete genome of an iridovirus isolated from the tiger frog. Virology **292:**185–197.
20. **Henley, J. R., E. W. Krueger, B. J. Oswald, and M. A. McNiven.** 1998. Dynamin-mediated internalization of caveolae. J. Cell Biol. **141:**85–99.
21. **Hernaez, B., and C. Alonso.** 2010. Dynamin- and clathrin-dependent endocytosis in African swine fever virus entry. J. Virol. **84:**2100–2109.
22. **Huang, H., et al.** 2006. Human herpesvirus 6 envelope cholesterol is required for virus entry. J. Gen. Virol. **87:**277–285.
23. **Inoue, Y., et al.** 2007. Clathrin-dependent entry of severe acute respiratory syndrome coronavirus into target cells expressing ACE2 with the cytoplasmic tail deleted. J. Virol. **81:**8722–8729.
24. **Jeonga, J. B., et al.** 2006. Molecular comparison of iridoviruses isolated from marine fish cultured in Korea and imported from China. Aquaculture **255:** 105–116.
25. **Jin, M., et al.** 2002. Hantaan virus enters cells by clathrin-dependent receptor-mediated endocytosis. Virology **294:**60–69.
26. **Kee, S. H., et al.** 2004. Effects of endocytosis inhibitory drugs on rubella virus entry into VeroE6 cells. Microbiol. Immunol. **48:**823–829.
27. **Kizhatil, K., and L. M. Albritton.** 1997. Requirements for different components of the host cell cytoskeleton distinguish ecotropic murine leukemia virus entry via endocytosis from entry via surface fusion. J. Virol. **71:**7145–7156.
28. **Klasse, P. J., R. Bron, and M. Marsh.** 1998. Mechanisms of enveloped virus entry into animal cells. Adv. Drug Deliv. Rev. **34:**65–91.
29. **Lamaze, C., et al.** 2001. Interleukin 2 receptors and detergent-resistant membrane domains define a clathrin-independent endocytic pathway. Mol. Cell **7:**661–671.
30. **Le, P. U., and I. R. Nabi.** 2003. Distinct caveolae-mediated endocytic pathways target the Golgi apparatus and the endoplasmic reticulum. J. Cell Sci. **116:**1059–1071.
31. **Luo, Y., et al.** 2009. Tiger frog virus can infect zebrafish cells for studying up- or down-regulated genes by proteomics approach. Virus Res. 171–179.
32. **Marsh, M., and A. Helenius.** 2006. Virus entry: open sesame. Cell **124:**729–740.
33. **Martinez, M. G., S. M. Cordo, and N. A. Candurra.** 2007. Characterization of Junin arenavirus cell entry. J. Gen. Virol. **88:**1776–1784.
34. **McAuslana1, B. R., and W. R. Smith.** 1968. Deoxyribonucleic acid synthesis in FV-3-infected mammalian cells. J. Virol. **2:**1006–1015.
35. **Minshall, R. D., et al.** 2000. Endothelial cell-surface gp60 activates vesicle formation and trafficking via G(i)-coupled Src kinase signaling pathway. J. Cell Biol. **150:**1057–1070.
36. **Morikawa, R. K., et al.** 2009. Intracellular phospholipase A1gamma (iPLA1gamma) is a novel factor involved in coat protein complex I- and Rab6-independent retrograde transport between the endoplasmic reticulum and the Golgi complex. J. Biol. Chem. **284:**26620–26630.
37. **Nabi, I. R., and P. U. Le.** 2003. Caveolae/raft-dependent endocytosis. J. Cell Biol. **161:**673–677.
38. **Newton, A. J., T. Kirchhausen, and V. N. Murthy.** 2006. Inhibition of dynamin completely blocks compensatory synaptic vesicle endocytosis. Proc. Natl. Acad. Sci. U. S. A. **103:**17955–17960.
39. **Nichols, B.** 2003. Caveosomes and endocytosis of lipid rafts. J. Cell Sci. **116:**4707–4714.
40. **Nichols, B. J.** 2002. A distinct class of endosome mediates clathrin-independent endocytosis to the Golgi complex. Nat. Cell Biol. **4:**374–378.
41. **Nomura, R., et al.** 2004. Human coronavirus 229E binds to CD13 in rafts and enters the cell through caveolae. J. Virol. **78:**8701–8718.
42. **O'Donnell, V., M. Larocco, and B. Baxt.** 2008. Heparan sulfate-binding foot-and-mouth disease virus enters cells via caveola-mediated endocytosis. J. Virol. **82:**9075–9085.
43. **Orlandi, P. A., and P. H. Fishman.** 1998. Filipin-dependent inhibition of cholera toxin: evidence for toxin internalization and activation through caveolae-like domains. J. Cell Biol. **141:**905–915.
44. **Pelkmans, L., and A. Helenius.** 2003. Insider information: what viruses tell us about endocytosis. Curr. Opin. Cell Biol. **15:**414–422.
45. **Pelkmans, L., J. Kartenbeck, and A. Helenius.** 2001. Caveolar endocytosis of simian virus 40 reveals a new two-step vesicular-transport pathway to the ER. Nat. Cell Biol. **3:**473–483.
46. **Pelkmans, L., D. Püntener, and A. Helenius.** 2002. Local actin polymerization and dynamin recruitment in SV40-induced internalization of caveolae. Science **296:**535–539.
47. **Peng, T., et al.** 2009. Entry of dengue virus serotype 2 into ECV304 cells depends on clathrin-dependent endocytosis, but not on caveolae-dependent endocytosis. Can. J. Microbiol. **55:**139–145.
48. **Perret, E., A. Lakkaraju, S. Deborde, R. Schreiner, and E. Rodriguez-Boulan.** 2005. Evolving endosomes: how many varieties and why? Curr. Opin. Cell Biol. **17:**423–434.
49. **Pho, M. T., A. Ashok, and W. J. Atwood.** 2000. JC virus enters human glial cells by clathrin-dependent receptor-mediated endocytosis. J. Virol. **74:** 2288–2292.
50. **Pietiäinen, V. M., V. Marjomäki, J. Heino, and T. Hyypiä.** 2005. Viral entry, lipid rafts and caveosomes. Ann. Med. **37:**394–403.
51. **Querbes, W., A. Benmerah, D. Tosoni, P. P. Di Fiore, and W. J. Atwood.** 2004. A JC virus-induced signal is required for infection of glial cells by a clathrin- and eps15-dependent pathway. J. Virol. **78:**250–256.
52. **Sánchez-San Martín, C., T. López, C. F. Arias, and S. López.** 2004. Characterization of rotavirus cell entry. J. Virol. **78:**2310–2318.
53. **Sieczkarski, S. B., and G. R. Whittaker.** 2002. Influenza virus can enter and infect cells in the absence of clathrin-mediated endocytosis. J. Virol. **76:** 10455–10464.
54. **Singh, R. D., et al.** 2006. Caveolar endocytosis and microdomain association of a glycosphingolipid analog is dependent on its sphingosine stereochemistry. J. Biol. Chem. **281:**30660–30668.
55. **Snyers, L., H. Zwickl, and D. Blaas.** 2003. Human rhinovirus type 2 is internalized by clathrin-mediated endocytosis. J. Virol. **77:**5360–5369.
56. **Stuart, A. D., and T. D. Brown.** 2006. Entry of feline calicivirus is dependent on clathrin-mediated endocytosis and acidification in endosomes. J. Virol. **80:**7500–7509.
57. **Stuart, A. D., H. E. Eustace, T. A. McKee, and T. D. Brown.** 2002. A novel cell entry pathway for a DAF-using human enterovirus is dependent on lipid rafts. J. Virol. **76:**9307–9322.
58. **Sun, X., V. K. Yau, B. J. Briggs, and G. R. Whittaker.** 2005. Role of clathrin-mediated endocytosis during vesicular stomatitis virus entry into host cells. Virology **338:**53–60.
59. **Tan, W. G., T. J. Barkman, V. Gregory Chinchar, and K. Essani.** 2004. Comparative genomic analyses of frog virus 3, type species of the genus *Ranavirus* (family *Iridoviridae*). Virology **323:**70–84.
60. **Tebar, F., T. Sorkina, A. Sorkin, M. Ericsson, and T. Kirchhausen.** 1996. Eps15 is a component of clathrin-coated pits and vesicles and is located at the rim of coated pits. J. Biol. Chem. **271:**28727–28730.
61. **Thomas, C. M., and E. J. Smart.** 2008. Caveolae structure and function. J. Cell. Mol. Med. **12:**796–809.
62. **Thomsen, P., K. Roepstorff, M. Stahlhut, and B. van Deurs.** 2002. Caveolae are highly immobile plasma membrane microdomains, which are not involved in constitutive endocytic trafficking. Mol. Biol. Cell **13:**238–250.
63. **Vidricaire, G., and M. J. Tremblay.** 2007. A clathrin, caveolae, and dynamin-independent endocytic pathway requiring free membrane cholesterol drives HIV-1 internalization and infection in polarized trophoblastic cells. J. Mol. Biol. **368:**1267–1283.
64. **Wang, Q., et al.** 2008. Identification of two novel membrane proteins from the Tiger frog virus (TFV). Virus Res. **136:**35–42.
65. **Weng, S. P., et al.** 2002. Outbreaks of an iridovirus disease in cultured tiger frog, Rana tigrina rugulosa, in southern China. J. Fish Dis. **25:**423–427.
66. **White, J., K. Matlin, and A. Helenius.** 1981. Cell fusion by Semliki Forest, influenza, and vesicular stomatitis viruses. J. Cell Biol. **89:**674–679.
67. **Whitley, D. S., et al.** 2010. Frog virus 3 ORF 53R, a putative myristoylated membrane protein, is essential for virus replication in vitro. Virology **405:** 448–456.
68. **Williams, T., V. Barbosa-Solomieu, and V. G. Chinchar.** 2005. A decade of advances in iridovirus research. Adv. Virus. Res. **65:**173–248.